Low-Temperature Exothermic Reactions in Al/CuO Nanothermites Producing Copper Nanodots and Accelerating Combustion

Mehnaz Mursalat, Ci Huang, Baptiste Julien, Mirko Schoenitz, Alain Estève, Carole Rossi, Edward L Dreizin

HAL Id: hal-03179381
https://laas.hal.science/hal-03179381

Submitted on 24 Mar 2021

Article

Low-Temperature Exothermic Reactions in Al/CuO Nanothermites Producing Copper Nanodots and Accelerating Combustion

Mehnaz Mursalat, Ci Huang, Baptiste Julien, Mirko Schoenitz, Alain Esteve, Carole Rossi, and Edward L. Dreizin*

Cite This: https://doi.org/10.1021/acsanm.1c00236

Read Online

ACCESS | Metrics & More | Article Recommendations | Supporting Information

ABSTRACT: Several Al/CuO nanocomposite reactive materials, prepared recently by arrested reactive milling, were found to exhibit a distinct low-temperature exothermic peak around 600 K seen by differential scanning calorimetry. This work is an experimental study aimed to establish whether this low-temperature reaction affects combustion and why it is observed in some but not all materials with identical compositions. The peak is only observed when aluminum is initially separately milled in acetonitrile. Electron microscopy showed resulting composite powders to be porous, unlike fully dense powders obtained without premilling aluminum. The as-prepared and partially reacted powders recovered after heating just past the peak to 650 K were examined using high-angle annular dark-field scanning transmission electron microscopy and electron energy loss spectroscopy. Additionally, X-ray diffraction measurements were performed for all materials. Finally, the reactive powders were ignited using plasma and shock generated by an electrostatic discharge. Results show that the low-temperature exothermic peak is associated with a redox reaction pathway involving release of oxygen by CuO that is not in direct contact with Al and free-molecular transport of that oxygen to the nearby surface of Al. This reaction pathway inhibits the formation of Al/Cu intermetallic phases. Instead, nanometer-scale metallic Cu particles are formed due to CuO reduction. It is also found that this reaction pathway accelerates ignition of reactive powders, which in turn leads to a higher burn rate of aerosolized powder.
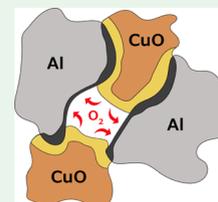
KEYWORDS: *redox reaction, metal combustion, energetic materials, heterogeneous kinetics, nanocomposite*

1. INTRODUCTION

Al/CuO nanothermites have been the subject of many recent studies because of their high energy density and transient gas combustion products attractive for many applications in pyrotechnics and other energetic formulations.[1−4] Different preparation methods, including mixing nanopowders,[5] electrospray assembly,[6−8] vacuum layer deposition,[9−13] electrochemical synthesis,[14] sol−gel processing,[15] self-assembly,[16−18] and arrested reactive milling (ARM),[19,20] were used to prepare such thermites, in which Al and CuO were mixed at the nanoscale. Despite similar scale of mixing, different methods (or even different variants of the same method) yield materials in which interfaces between reactive components have different structures and characteristics. Such differences are expected to affect the ignition and combustion of the nanothermites; thus, modifying the reactive interfaces could be an effective way of controlling reactions in nanothermites even if their chemical compositions remain the same.[21−23]

Vacuum layer deposition offers the most ordered (often planar) interface structures and direct methods of tuning the chemical properties of the produced interfaces, that is, by altering the sequence in which the layers are grown or by embedding sublayers or inclusions.[24,25] For example, nano-inclusions of gold resulted in corrugated layers and altered the redox reaction.[25] Differential scanning calorimetry (DSC) showed an unusual, distinct low-temperature exothermic peak around 600 K. It was attributed to accelerated decomposition of CuO in the presence of surface defects at the CuO/Al interface. A similar low-temperature exothermic peak was reported for vacuum-deposited Al/CuO nanofoils when a thin intermediate Cu layer was added.[26] In the latter case, the Cu layer was thought to prevent evaporation of Cu during combustion but was proposed to not offer a substantial obstacle for gaseous oxygen formed during CuO decomposition. In a related work, it was observed that the process control agents (PCAs) used for ARM, such as stearic acid, hexane, or acetonitrile, affect the reactive behavior of nanocomposite powders prepared by ARM,[27−29] likely by altering the interface properties. In a recent study,[30] nanothermites with 8/3 molar Al/CuO ratio (equivalence ratio 4) were prepared by ARM with hexane serving as PCA while using Al and/or CuO powders preliminarily milled in acetonitrile. Like for the modified nanofoils,[25,26] DSC traces for some of these composite powders showed distinct exothermic reactions near 600 K. This reaction was only observed for nanothermites using Al powder that was premilled in acetonitrile. In materials prepared with as-received

(not premilled) aluminum, the low-temperature reactions are represented by a broad, relatively flat signal with no peak around 600 K; additionally, an endotherm indicative of Al/Al$_2$Cu eutectic is observed before the main redox reaction occurring at ≈850 K. These previous results for xAl/yCuO (x and y representing respective mole parts) nanofoils and nanocomposite powders are summarized in Figure 1. It was also reported that the nanocomposite powders exhibiting the low-temperature DSC peak ignited at a reduced temperature when coated on an electrically heated wire.[30]
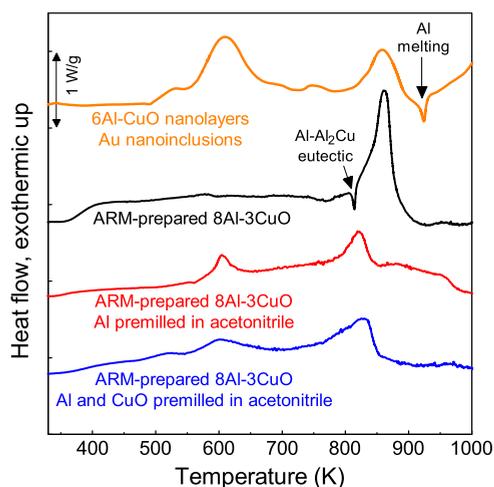

Figure 1. Previously reported DSC curves for Al/CuO nanofoils with Au nanoinclusions (top curve, equivalence ratio 9, heating rate 20 K/min)[25] and Al/CuO nanocomposite powders prepared by ARM[30] (bottom three curves, equivalence ratio 4, heating rate 5 K/min).

The goal of the present study is to determine whether the low-temperature exothermic reactions detected in the nanothermites with altered interfaces prepared by ARM affect their bulk burn rates. It is further of interest to understand the nature of the low-temperature exothermic reactions observed when aluminum premilled in acetonitrile is used to prepare the nanocomposite powders. To that end, it is necessary to characterize the reaction products generated by these unique low-temperature exothermic processes.

2. EXPERIMENTAL SECTION

2.1. Reactive Composite Powders. Materials used in this work, 8Al·3CuO powders (respective 8/3 mole ratio), are the same as prepared in ref 30. This metal-rich composition is expected to be of interest when thermite reaction can be augmented by combustion of the excess Al in the ambient gaseous oxidizer.

Briefly, −325 mesh 99.5% pure aluminum (Atlantic Equipment Engineers) and 10 μm 99+% pure copper(II) oxide (Sigma-Aldrich) served as the starting components. For the relatively coarse aluminum used, the common 2−4 nm thick layer of natural alumina makes up only a fraction of a percent of the powder volume, so that no correction is necessary to account for its effect on the active aluminum content. PCAs were either 95% pure hexane (Alfa Aesar) or 99.5% pure acetonitrile by Alfa Aesar. A Retsch PM400 planetary mill operated at 350 rpm was used with custom-made 175 mL milling vials capable of withstanding high pressure that could develop in case of accidental mechanical initiation of the milled thermite. Powder load per vial was 30 g; 3/8 in (9.53 mm) hardened steel balls were used; the ball to powder mass ratio was 3. A diagram illustrating the milling sequence used to prepare powders is shown in Figure 2. Aside from the powder prepared in first stage milling using as-received Al and CuO with 24 mL of hexane as PCA, referred to as A-C- (see dashed arrows in Figure 2), two materials including premilled Al with as-received CuO (ApC-) and both premilled Al and CuO (ApCp) were prepared in two stages, including the initial milling step in acetonitrile. For each stage, the milling time was 60 min. After the first milling stage, the powders were dried in Ar for 24 h to remove any remaining acetonitrile. For the second stage milling, each vial was loaded with 14.25 g of Al and 15.75 g of CuO. All powders prepared for this study were stored in hexane. The material prepared from as-received Al and premilled CuO, referred to as A-Cp, was observed in ref 30 to behave qualitatively similar to A-C- and was therefore not included in the present study.

2.2. Material Characterization. Reactions occurring in the ARM-prepared nanocomposite thermite powders were characterized by DSC using a Netzsch STA409PC thermal analyzer. 15−20 mg of powders immersed in hexane were loaded in an alumina crucible in order to prevent oxidation and ignition during loading in air. Upon loading the crucible in the analyzer, the liquid was allowed to evaporate in argon (Airgas, 99.98%). Next, the furnace was evacuated and then flushed with argon three times before heating at 5 K/min to 800 °C under a 50 mL/min Ar flow. Note that the relatively high sample mass used here, established as safe in preliminary experiments, was chosen to increase the signal at relatively low temperatures. In general, caution should be taken to prevent accidental initiation during loading or as a result of fast heating to higher temperatures.

Phase composition was determined by X-ray diffraction (XRD) on a PANalytical Empyrean multipurpose research diffractometer
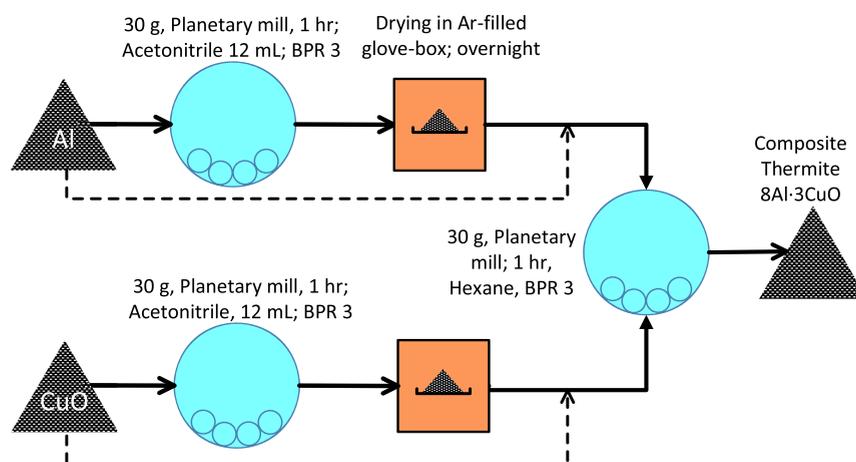

Figure 2. Two-stage milling procedure used to prepare nanocomposite thermite powders with premilled Al and/or CuO.
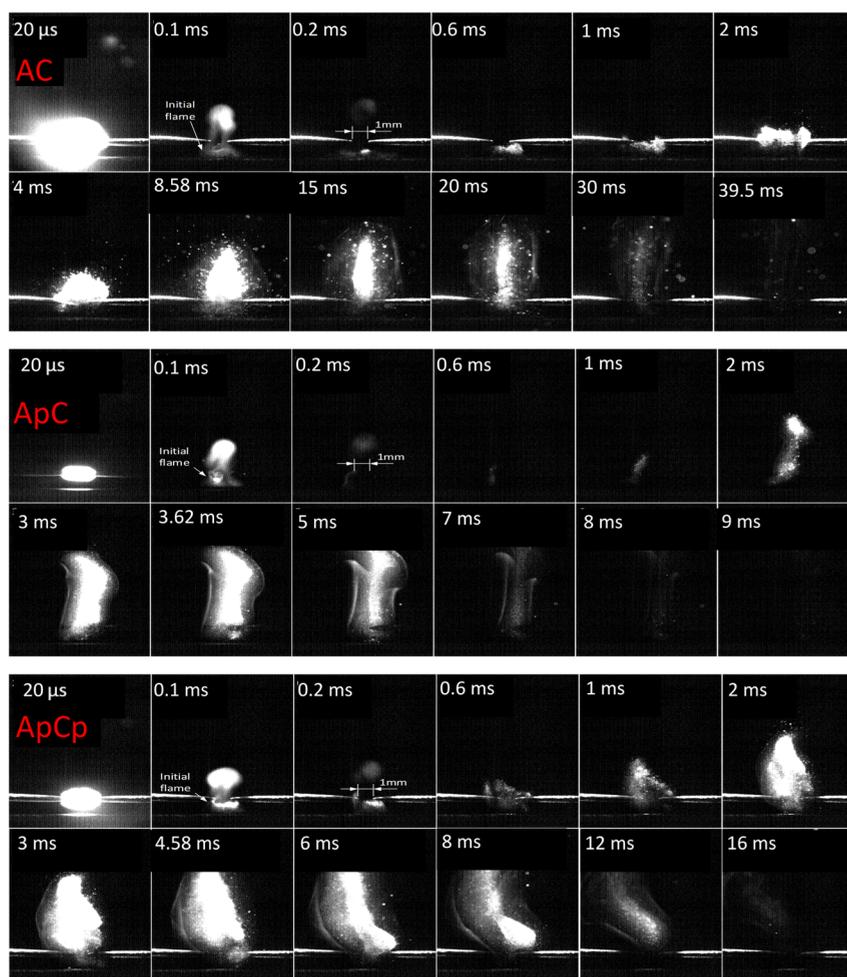
Figure 3. High-speed video frames showing the ESD-induced combustion of powders A-C-, ApC-, and ApCp on an aluminum substrate 1 mm below the electrode gap.

operated at 45 kV and 40 mA with unfiltered Cu Kα radiation (λ = 1.5438 Å). Phases were identified using the PDF-4+ database[31] and the tools built into the HighScore Plus software (version 3.0e)[32] for the whole-pattern refinement.

Morphology and chemical composition of the nanocomposite powders were analyzed by transmission electron microscopy (TEM), scanning TEM (STEM), and electron energy-loss spectroscopy (EELS) using a JEOL cold-FEG JEM-ARM200F operated at 200 kV equipped with a probe Cs corrector reaching a spatial resolution of 0.078 nm. EELS data were acquired on a Gatan Imaging Filter Quantum (energy resolution of 0.3 eV) using a dispersion of 0.5 eV/channel, a collection semiangle of 19.4 mrad, and a convergence semiangle of 14.8 mrad. The spatial resolution is estimated at 0.5 nm. STEM samples were prepared by ultramicrotomy, that is, the powders were embedded in epoxy resin (MA2+, Presi) before being cut in 50 nm slices, placed in Ni hexagonal grids, and then coated with a 20 nm carbon layer for analysis.

Electron probe microanalysis was also used to quantify the chemical composition of the powders using a Cameca SXFive FE microprobe operated at low voltage (7 kV) to have a sub-μm X-ray generation volume. Quantitative analysis was accomplished by comparing the intensities of characteristic X-rays for elemental Al, Cu, and O with respective intensities for standard natural minerals.

For combustion tests, the ARM-prepared powders were ignited in air by the shock and plasma produced by an electrostatic discharge (ESD) initiated near the sample. The ESD was produced using a model 931 Firing Test System by Electro-Tech Systems, Inc. A 10 nF capacitor charged to 20 kV and discharged between two pin-electrodes set 1 mm apart served to generate the ESD. Precision point

steel pins (0.9 mm diameter) by Super Steel Microground, Dritz were used as electrodes. A detailed description of the setup can be found elsewhere.[33] A Photron FASTCAM Nova high-speed camera (type: 800K-M-8GB) operated at 50,000 fps with an exposure time of 20 μs was used to capture the images of the ignited powder. Each recorded video includes 5 frames before the trigger signal and 4995 frames after the trigger, providing a time span of 100 ms. The camera was operated with a 0.7−4.5× Zoom Monocular lens by Hayear Corp. Ltd. An FL532-10 laser line filter by Thorlabs, ensuring only the passage of 532 ± 10 nm wavelength, was used to avoid saturation and to protect the image sensor in the camera. The camera was triggered by a pulse from an induction coil by Pearson Electronics (model 110A) measuring the ESD current.

The composite powder was placed in a recession in a 1.6 mm thick aluminum alloy (6061-T1) plate (by McMaster-Carr) about 1 mm below the pin electrodes. The recession with approximately 2.6 mm length, 0.4 mm width, and 0.4 mm depth was made on the plate by hammering a flat-tip screwdriver onto its surface. Approximately, 3−4 mg of the powder was loaded into the recession with a spatula. Using the tip of the spatula, any large lose agglomerates were broken. The powder surface was then flattened and excess powder removed with a glove-covered fingertip.

3. RESULTS

3.1. Combustion Experiments. Combustion of the differently prepared nanocomposite thermites (A-C-, ApC-, and ApCp) exposed to the shock and plasma produced by ESD includes events that are qualitatively similar to those reported

recently for zirconium powder, ignited using the same method.[34] For all powders, weak emission from igniting particles initiates effectively immediately. A much stronger combustion event is observed following a substantial delay on the order of 1 ms. Example sequences of the recorded high-speed videos are shown in Figure 3. The images were taken every 20 μs; only selected images are shown for each experiment. For each powder, at least five combustion runs were recorded and examined.

Differences in the emission produced by the initial (instant) flame immediately following the ESD are difficult to discern among different powders. However, differences in the dynamics and appearance of the delayed flames are clear. For A-C- powder, the flame appeared after a longer delay and existed longer than for either ApC- or ApCp powders. For the latter two powders, a faster flame propagation is also noted based on the recorded videos. Many individual particle streaks are observed for the flame produced by A-C- powder, whereas almost no such streaks are noted for either ApC- or ApCp powders. Flames produced by ApC- and ApCp powders comprise rather a uniform central core and a diffuse cloud with a sharp boundary, suggesting substantial gas release. A luminous cloud suggesting gas release can also be distinguished at later times for the A-C- powder flame; however, its boundary is fuzzy.

To quantify the differences between the combustion characteristics of different powders, the total emission intensity for each video frame is integrated over the entire field of view. Such integral intensity values are shown in Figure 4 as a
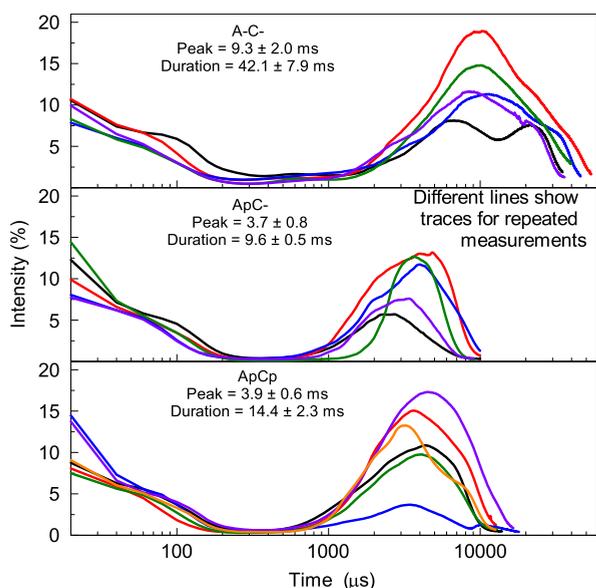

Figure 4. Integrated time-resolved emission traces obtained by processing the high-speed video frames for different powders A-C-, ApC-, and ApCp.

function of time and clearly show the development of the delayed flames. The initial decay, largely similar for all powders, is mostly caused by the diminishing emission produced by the plasma kernel associated with ESD. The characteristic time for such a decay is 200 μs. A larger peak appearing with ms delay is produced by the delayed powder flame. This peak appears later and lasts longer for A-C- powder compared to the peaks produced by burning ApC- and ApCp

powders. Thus, the powders exhibiting a distinct low-temperature exotherm in their DSC traces (Figure 1) also ignite sooner and burn faster.

The video frames were further processed to identify the flame height using image binarization.[35] For each tested powder, the flame height profiles were averaged among five tests. The results are shown in Figure 5. The flames propagate fastest for ApCp, followed by ApC- and then by A-C-.
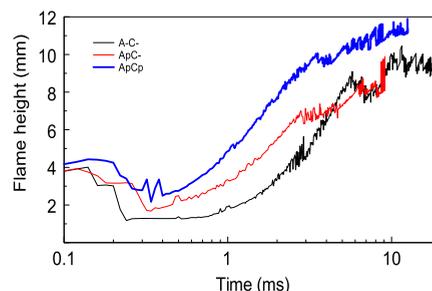

Figure 5. Time-resolved flame height profiles of A-C-, ApC-, and ApCp powder combustion by ESD. Each profile was average among at least five repetitions.

The ignition and combustion results clearly indicate that premilling Al has an effect on the reactive behavior of the Al/CuO nanocomposite powders. Powders prepared with premilled Al initiate sooner and burn faster than those made with regular Al, indicating a correlation between the low-temperature exothermic reaction and higher burn rates.

3.2. Morphology and Phase Analysis of Reactive Composite Powders. To determine how using premilled Al to prepare the nanothermite affects the low-temperature exothermic reaction, the morphology and microstructural and chemical features of the different Al/CuO nanocomposite powders were investigated. A-C-, ApC-, and ApCp powders were heated in the thermal analyzer to 650 K (end of the low-temperature exotherm, cf. Figure 1) under argon at a rate of 5 K/min (same conditions as DSC experiments) and recovered. The as-prepared and partially reacted powders were further analyzed using XRD and STEM. When necessary, complementary elemental compositions of powder phases were quantified using an electron microprobe.

3.2.1. Bulk Composition of the As-Prepared and Partially Reacted Powders. The XRD patterns for all as-prepared powders are shown in Supporting Information, Figure S1. They look qualitatively similar to one another with major peaks corresponding to aluminum and tenorite (a polymorph of CuO). Although amorphous Al_2O_3 may be difficult to detect by XRD, no trace of reduced crystalline species, such as Cu_2O or Cu, was found, suggesting that any reaction occurring during milling is negligible. XRD patterns for partially reacted powders recovered from 650 K are shown in Figure 6. Table S1 shows the compositions obtained from the whole pattern refinement. Cu_2O and Al_2Cu are the most abundant reaction products formed prior to 650 K. The amount of Al_2Cu in A-C- prepared without premilling Al is much higher than in other samples. The powder ApC- contains the greatest amount of unreduced CuO, which is readily understood, considering that this material contains a relatively large number of CuO particles that are not in immediate contact with Al[30] (discussed later).
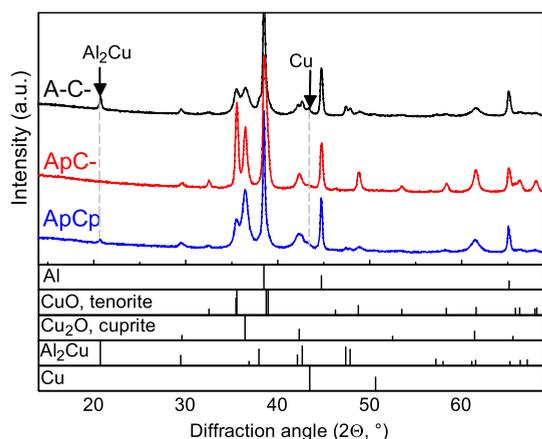
Figure 6. XRD patterns of ARM-prepared 8Al·3CuO thermite powders quenched from 650 K. The strongest peaks of Al₂Cu and Cu are indicated with arrows.

3.2.2. Near Surface and Interface Composition of the As-Prepared and Partially Reacted Powders. In complement to bulk XRD analysis, atomically resolved STEM−high-angle annular dark-field (HAADF) and STEM−EELS were performed in the ARM-prepared powder with premilled Al and as-received Al, that is, ApC- and A-C-, in as-prepared condition and after recovering from 650 K. EELS here is used to monitor the evolution of the oxidation state of Cu and Al oxides in order to unravel the reaction pathway associated with the low-temperature exothermic reaction seen in ApC- powders. Hence, electron loss near edge structure (ELNES) of Cu L$_{2,3}$-edges@932−953 eV, O K-edges@532 eV, and Al K edges@1560 eV were acquired on different zones near and across Al/CuO interfaces. EELS core loss edges were background subtracted using a power law fit before being plotted.

The ELNES of the Cu oxides in both A-C- and ApC- as-prepared powders is characterized by sharp and symmetric peaks at 932 eV L₃ (2p$_{3/2}$ → 3d) and 953 eV L₂ (2p$_{1/2}$ → 3d) lines which correspond to cupric oxide (Figure 7). No CuO reduction is observed near surfaces for both as-prepared powders. Elemental composition quantified by an electron microprobe confirmed the EELS analyses: CuO phases are composed of 49 ± 1% of O and 50 ± 1% of Cu.

However, differences between Al-bearing phases are detected for samples prepared using as-received and premilled Al. In A-C- powders, pure Al is detected (gray lines in ELNES spectra of Figure 7a,b) and Al oxide is only present in contact with CuO, unlike ApC- powders in which Al is oxidized over a much thicker zone (≈30 nm measured in ELNES spectra of Figure 7c). Quantification of the oxygen content in Al by the electron microprobe gave 9 ± 1% of O and 91 ± 1% of Al.

Finally, both as-prepared materials, A-C- and ApC-, form interfacial layers made of atomic mixture of Al, Cu, and O (yellow lines in the spectra of Figure 7).

After heating to 650 K and the respective partial reaction, there is a clear evolution in both microstructures and EELS signatures. The STEM−HAADF image of ApC- (Figure 8) gives direct evidence of formation of copper dots (5−10 nm in dimension) in the AlO$_x$ phase. The Cu-L$_{2,3}$ edge spectra acquired across a dot (in Supporting Information, Figure S2) confirms the sole presence of Cu. Neither oxygen nor Al is detected in the dots.

In contrast, in these analyses targeting surfaces of the particles for partially reacted A-C- powders, no pure copper but cuprous oxide is detected (Figure 9a) close to AlO$_x$ zones. Looking in detail at the interfacial zone, pre-edge O K peaks at 530 eV were observed (Figure 9b) which reveal the presence of gaseous oxygen that could have liberated from the decomposing CuO upon heating and accumulated at the interface.[36] Finally, we also see in quenched A-C- the growth of an intermetallic phase (yellow lines in ELNES spectra of Figure 9b) which is consistent with both XRD (Figure 6) and DSC analyses (Figure 1, presence of the endotherm at ≈820 K).

4. DISCUSSION

Differences in the morphology of the Al/CuO interface induced by premilling Al in acetonitrile were observed to affect the low-temperature reaction mechanism in the nano-composite thermites and subsequent reactivity. To interpret the present results, it should be first recognized that a continuous range of interfaces with different structures is present in all nanocomposites prepared by ARM. Scanning electron microscopy (SEM) results reported elsewhere[30] consistently with the present STEM work suggest a near full-density mixing between Al and CuO for A-C- powders, whereas fully dense composite structures are combined with porous particles in ApC- and ApCp powders. This is confirmed by SEM images of the as-prepared powder samples for microprobe analysis (in Supporting Information, Figure S3) showing differences in reactant intimacy and CuO distribution when Al is premilled: CuO and Al are mixed intimately in A-C- powders, whereas porosity is observed in ApC- powders with Al and CuO separated from each other. The presence of these nanovoids between Al and CuO phases modifies the low-temperature reaction pathway as evidenced by DSC and supported by STEM−EELS results (Section 3.2). Paradoxi-cally, separation of Al and CuO by nanovoids forming in ApC- and ApCp powders accelerates the low-temperature reaction and leads to the complete reduction of CuO to metallic Cu (yielding the observed Cu nanodots), at least close to the particle surface. The mechanisms of such reactions are qualitatively discussed below.

In a fully dense nanocomposite, the reaction occurs at the CuO/Al₂O₃ interface and is controlled by diffusion of ions of Al through the growing layer of Al₂O₃ as was proposed earlier.[37] Indeed, transport of Al directly to CuO explains the formation of greater amounts of Al₂Cu detected in the products (Figure 6 and Table S1) and the eutectic melting peak observed only for the A-C- material in Figure 1. Counter diffusion of oxygen from decomposing CuO must be slower. If the reaction occurred at the Al/Al₂O₃ interface, Al and Cu would always be separated by a layer of Al₂O₃ preventing formation of the alloys. The schematic diagram in Figure 10a shows the above discussed reaction in fully dense composites. For simplicity, such composites are shown as planar layers. Initially Al and CuO are not separated by an oxide layer. This is because during high-energy milling, a new pristine surface of aluminum is produced and pressed against copper oxide without the formation of a passivation layer. Any alumina remaining from the starting Al powder is redistributed during milling and not systematically present at the Al/CuO interface.

Initially, CuO is reduced to Cu₂O, as supported by STEM−EELS (Figure 9a,b), which detect cuprous oxides and gaseous oxygen trapped near Al/CuO interface in A-C- powders after partial reaction and recovery from 650 K. Continuing reaction
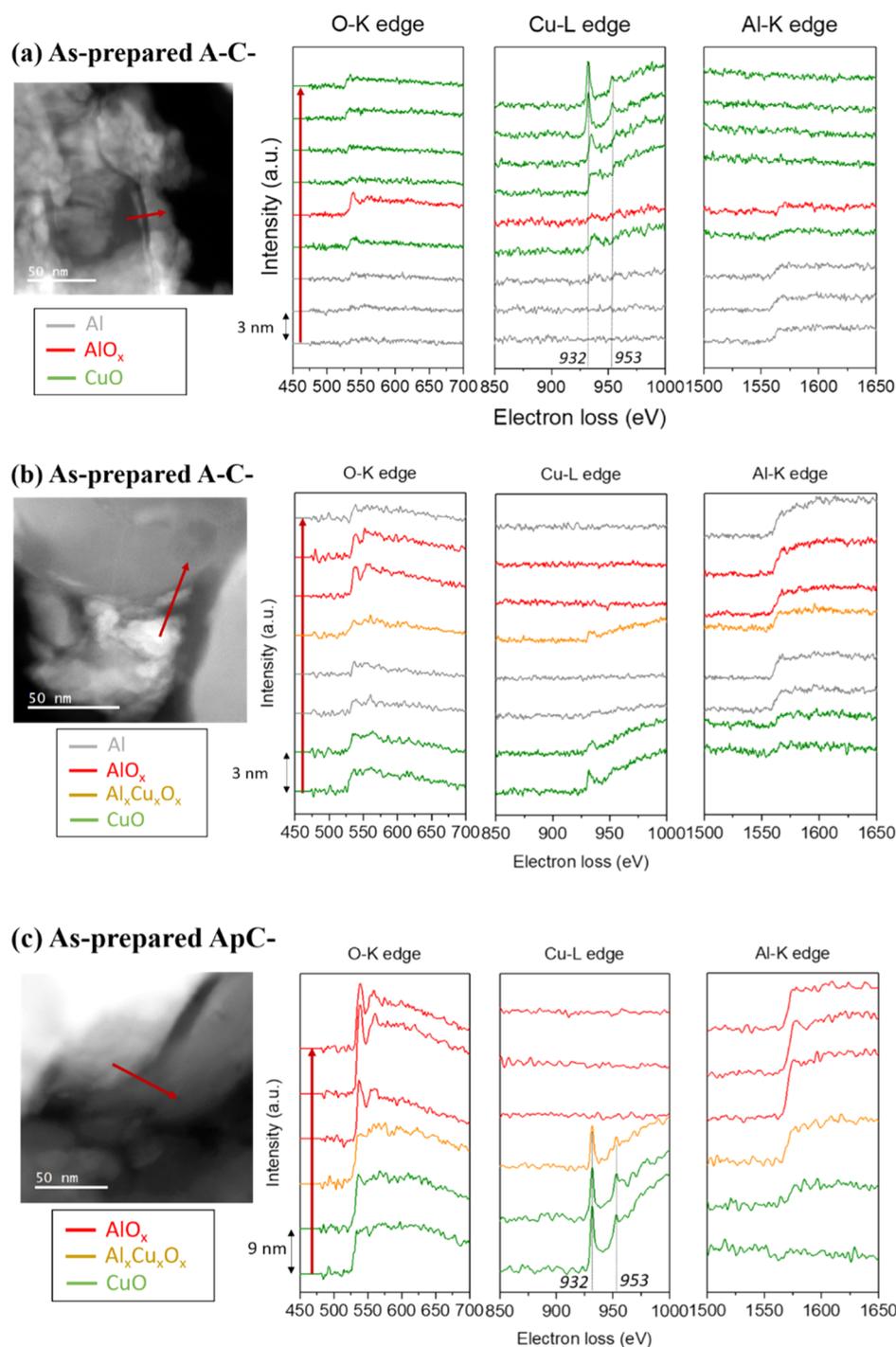
Figure 7. As prepared samples: cross-sectional STEM−HAADF images and ELNES spectra of Cu $L_{2,3}$-edge, Al $L_{2,3}$-edge, and O K-edge acquired across (a) Al/CuO interface and (b) CuO/Al interface in A-C- and (c) CuO/Al interface in ApC-. EELS spectra were acquired every 1 nm but plotted every 3 nm for (a,b) and 9 nm for (c).

causes formation of Al/Cu intermetallic inclusions along the Al_2O_3/Cu_2O interface (observed in STEM−EELS diagrams in Figure 9b). This is the proposed reaction scenario for the fully dense A-C- powders.

The same reaction can occur in ApC- and ApCp powders for the part of the material, in which CuO is in intimate contact with Al. However, because part of CuO is separated from Al (or Al_2O_3 covering Al surface), as shown in Figure 10b, an alternative reaction pathway becomes available. The schematic simplifies the structure, assuming it to be similar to that of the fully dense material but including parts of CuO surfaces that are not in contact with Al or Al_2O_3. Clearly, different geometries are possible having the common feature of CuO surface slightly removed from Al. Upon heating, CuO begins to decompose releasing oxygen. This oxygen must be transferred through the voids to the nearby surfaces of Al_2O_3. It then can react with Al ions diffusing outward to the Al_2O_3/gas interface.[38] If such a reaction continues, the CuO domain that released oxygen can be reduced to metallic Cu, completely avoiding the formation of Al/Cu intermetallics. This can
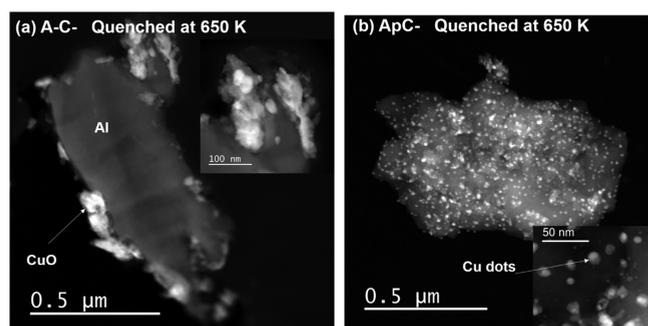
(a) A-C- Quenched at 650 K

Al

CuO

0.5 μm

100 nm

(b) ApC- Quenched at 650 K

Cu dots

0.5 μm

50 nm

Figure 8. Samples heated to and recovered from 650 K: cross-sectional STEM−HAADF images of A-C- and ApC- materials. The insets in (a,b) show a magnified view.

explain the formation of multiple Cu nanodots embedded into alumina observed to form by 650 K on the surface of both ApC- and ApCp powders (Figure 8 and in Supporting Information Figure S4), which include significant portion of CuO that is not in direct contact with Al. The rate of the reaction described here depends on how fast oxygen released by CuO can be transported across the void separating it from Al. In the present material, such voids have dimensions of 10−100 nm, which are comparable or less than the mean free path of the gas molecules at the temperatures of interest. Thus, gas phase diffusion is not a factor affecting the reaction rate. Instead, oxygen released by decomposing CuO is transported in the free molecular regime to Al ions at the surface of Al_2O_3, where it is immediately consumed. In this case, CuO behaves as if it is exposed to high vacuum, so that its decomposition is accelerated.
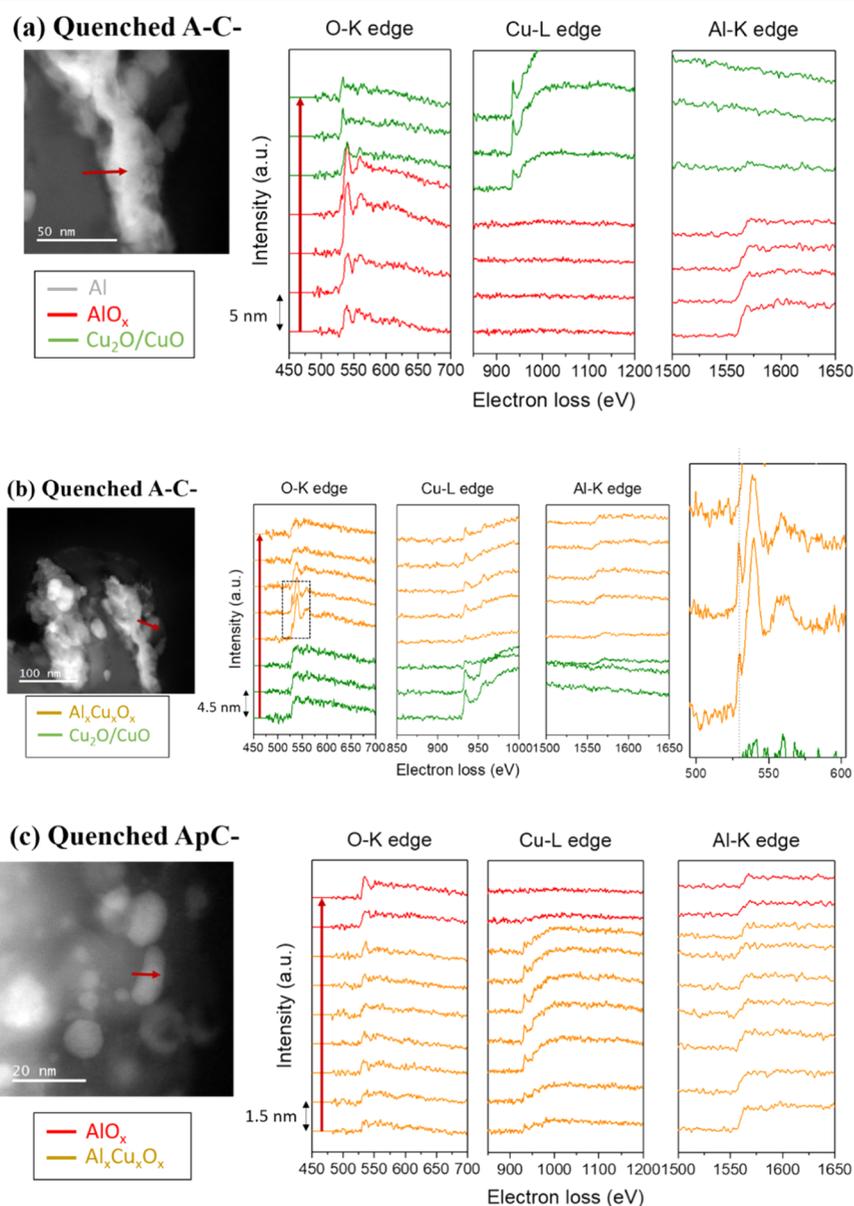

Figure 9. Samples heated to and recovered from 650 K: cross-sectional STEM−HAADF images and ELNES spectra of Cu $L_{2,3}$-edge, Al $L_{2,3}$-edge, and O K-edge acquired across (a) AlO_x/Cu_2O in quenched A-C-, (b) Cu_2O/AlO_x interface showing a pre-edge O K peak at 530 eV in quenched A-C-, and (c) across a ApC zone being reacted. EELS spectra were acquired every 0.5 nm but plotted every 5, 4.5, and 9 nm for analysis (a−c), respectively.
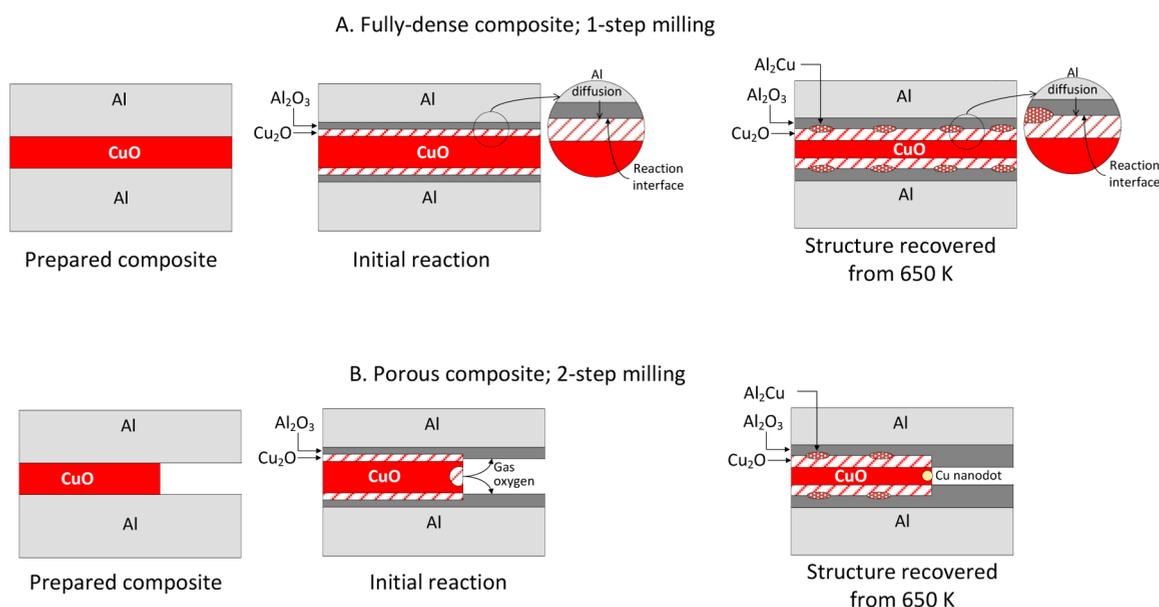
Figure 10. Schematic diagram illustrating the low-temperature redox reactions and formation of products in the fully dense composite (A) and in the porous composite (B).

As noted above, the morphology illustrated schematically in Figure 10b is just an example; any CuO particle or inclusion having an exposed surface in the vicinity of Al can be precursor to one or more Cu nanodots. Based on the present experimental observations, it is proposed that the redox reaction occurring via release of oxygen from CuO that oxidizes Al at the nearby exposed Al_2O_3 surface explains the formation of the low-temperature peak observed in Figure 1. No gaseous oxygen was detected in STEM–EELS of quenched ApC- powders, suggesting that all such oxygen released in the voids reacted readily upon adsorbing to the Al or Al_2O_3 surface. This is consistent with the STEM–EELS analysis shown in Figure 7c which reveals slightly oxidized aluminum (8% O and 92% Al) in ApC- near the Al/CuO interface. Conversely, observed traces of gaseous oxygen for A-C- suggest that Al is oxidized at the Al_2O_3/CuO (or Cu_2O) interface and not at the Al_2O_3 part exposed to gas (where there is no nearby decomposing CuO surface).

The proposed reaction mechanism involving free-molecular transport of oxygen released by CuO into nanovoids may be dominant, at least at low temperatures, for powders containing CuO and Al_2O_3 surfaces that are not in direct contact with each other, while the separation between such surfaces remains sufficiently small. The predominant nature of such a reaction is consistent with the STEM observations suggesting the presence of Cu_2O near the surface of the A-C- powders but only detecting elemental Cu for the ApC- powders (STEM–EELS spectra in Figure 9). Oxygen leaving the condensed phase and entering the pore space in measurable quantities is further supported by previous observations of oxygenated gas release near 600 K observed by thermogravimetry with coupled mass spectrometry in similar 8Al·3CuO nanocomposites prepared by a related ARM technique.[39] Interestingly, gas release accompanying ignition has also been observed previously for similar Al·CuO thermites prepared by milling and heated much faster than in the present thermo-analytical experiments.[40] Additional work is desired, further characterizing and quantifying such gas release due to CuO decomposition occurring in different experimental configurations.

Because separating CuO from Al removes the kinetic pathway enabling formation of intermetallics, it leads to a reaction producing only Al_2O_3 and Cu, which is more thermodynamically favored compared to that producing additionally Cu_2O and Al/Cu intermetallics. On the other hand, this reaction may begin at a higher temperature because it requires release of oxygen by CuO. Conversely, in fully dense systems, Al diffusing to CuO may begin reacting directly with condensed CuO before any oxygen is released. Thus, when the temperature is sufficiently high for CuO to begin releasing oxygen, the reaction that started earlier in the fully dense systems may have led to growth of a thicker alumina layer (see reaction for A-C-, schematically represented by Figure 10a) compared to the case with CuO separated from Al. A thicker alumina layer in the fully dense thermites thus serves to slow down the reaction at higher temperatures, when release of gas oxygen by CuO begins. Conversely, the lack of very low-temperature condensed phase reaction in materials containing nanovoids leads to a greater redox reaction rate when the temperature increases to trigger release of oxygen by CuO. This explains a relatively sharp peak observed for such materials in DSC (Figure 1).

The same mechanism can also be applied to describe the low-temperature exothermic reaction observed in Al/CuO nanolayers with embedded gold nanoparticles (see Figure 1).[25] Indeed, it was observed that multiple defects were formed around such nanoparticles upon heating, causing voids around the Al/CuO interface. It is proposed here that the presence of voids generated due to heating of a corrugated interface led to separation of Al (and growing Al_2O_3) from CuO, thus prompting release of gaseous oxygen reacting with Al. Interestingly, Cu nanodots were not detected in ref 25, where electron microscopy was done with cross-sectioned multilayered structures, making it difficult to resolve the nanodots that might have formed on the surface of growing voids.

It is further interesting that the low-temperature reactions detected in DSC measurements and causing the formation of Cu nanodots discussed above appear to affect combustion of

the nanocomposite powders, as implied from the reported experiments (Figures 3−5). Both qualitative differences in the flame appearance and quantitative differences in the flame propagation and the bulk burn rate suggest that the low-temperature reactions lead to an accelerated ignition and faster combustion. Because combustion of these Al-rich thermites involves much higher temperatures (typically, >2000 K) than those relevant to the discussed exothermic reactions, it is suggested that the observed bulk effect on the burn rate is due to an earlier ignition of the composite particles. An earlier ignition accelerates the heat release, which in turn can further accelerate combustion of the aerosolized powders tested here. In other words, the effect is unlikely to be detectable when single particle burn times are measured in experiments, in which combustion of each particle occurs independently. Conversely, for collective combustion of multiple interacting particles, the acceleration of the bulk burn rate can be significant.

5. CONCLUSIONS

In this work, atomically resolved STEM−HAADF and STEM−EELS were performed on reactive nanocomposite powders prepared by ARM using Al premilled in acetonitrile and unmodified Al. The as-prepared and partially reacted materials were analyzed in order to unravel their low-temperature reaction pathway. In the fully dense material prepared with unmodified Al, the reaction occurs at the Al_2O_3/CuO interface where gaseous oxygen is trapped after CuO decomposition. This causes the formation of Al/Cu intermetallic inclusions along the Al_2O_3/Cu_2O interface. When Al is premilled in acetonitrile, the prepared Al/CuO powders contain nanosized pores. Separating Al and CuO phases modifies the reaction pathway involving the formation of gaseous oxygen by reduced CuO that is not in direct contact with Al. The generated gaseous oxygen moves, in free-molecular regime, through the nanovoids to nearby surfaces of Al_2O_3/Al grains where it reacts with Al diffusing outward through the formed oxide layer. The reaction continues, that is, the CuO domain around the voids is reduced to metallic Cu. Thus, somewhat unexpectedly, the introduced small separation between Al and CuO removes the kinetic pathway, enabling the formation of Al/Cu intermetallic phases as a byproduct of the redox reaction. This leads to a more thermodynamically preferred scenario yielding only Al_2O_3 and Cu. This reaction triggered by the release of oxygen by CuO begins at slightly higher temperatures than that proceeding in the fully dense phase with Al reaching CuO directly by diffusion through Al_2O_3. Because the redox reaction in the material containing nanovoids is delayed to higher temperatures, once started, it proceeds faster because of a thinner pre-existing layer of Al_2O_3. This explains the relatively sharp low-temperature exothermic peak observed by DSC of Al/CuO powders prepared with Al premilled in acetonitrile. Once such reaction pathway is enabled, the ignition delays of reactive material particles are reduced, and the bulk burn rate is increased. This work emphasizes the major role of the interface structure between reactive components in controlling reactions in nanothermites.

ASSOCIATED CONTENT

Ⓢ Supporting Information

The Supporting Information is available free of charge at https://pubs.acs.org/doi/10.1021/acsanm.1c00236.

Phase composition in wt-% of materials recovered from 650 K; X-ray diffraction patterns for different prepared composite powders; TEM image and respective Cu-L2,3 edge spectra characterizing the copper dots; SEM images of samples prepared for the microprobe analysis; and cross-sectional STEM-HAADF image of the sample developing copper nanodots after being heated to and recovered from 650 K (PDF)

AUTHOR INFORMATION

Corresponding Author

Edward L. Dreizin − New Jersey Institute of Technology, Newark, New Jersey 07103, United States; orcid.org/0000-0003-0859-0984; Email: dreizin@njit.edu

Authors

Mehnaz Mursalat − New Jersey Institute of Technology, Newark, New Jersey 07103, United States

Ci Huang − New Jersey Institute of Technology, Newark, New Jersey 07103, United States

Baptiste Julien − LAAS-CNRS, University of Toulouse, 31400 Toulouse, France

Mirko Schoenitz − New Jersey Institute of Technology, Newark, New Jersey 07103, United States; orcid.org/0000-0002-9142-8162

Alain Esteve − LAAS-CNRS, University of Toulouse, 31400 Toulouse, France; orcid.org/0000-0002-0301-7479

Carole Rossi − LAAS-CNRS, University of Toulouse, 31400 Toulouse, France; orcid.org/0000-0003-3864-7574

Complete contact information is available at:
https://pubs.acs.org/10.1021/acsanm.1c00236

Notes

The authors declare no competing financial interest.

REFERENCES

(1) Coffey, B.; Schropp, D. R.; Kwiatkowski, K. C. Solid-state thermite composition based heating device. US Patent 20100252022 A1, 2010.

(2) Yetter, R. A.; Risha, G. A.; Son, S. F. Metal particle combustion and nanotechnology. Proc. Combust. Inst. 2009, 32, 1819−1838.

(3) Lanthony, C.; Guiltat, M.; Ducéré, J. M.; Verdier, A.; Hémeryck, A.; Djafari-Rouhani, M.; Rossi, C.; Chabal, Y. J.; Estève, A. Elementary Surface Chemistry during CuO/Al Nanolaminate-Thermite Synthesis: Copper and Oxygen Deposition on Aluminum (111) Surfaces. ACS Appl. Mater. Interfaces 2014, 6, 15086−15097.

(4) Rossi, C.; Zhang, K.; Esteve, D.; Alphonse, P.; Tailhades, P.; Vahlas, C. Nanoenergetic Materials for MEMS: A Review. J. Microelectromech. Syst. 2007, 16, 919−931.

(5) Puszynski, J. A.; Bulian, C. J.; Swiatkiewicz, J. J. The effect of nanopowder attributes on reaction mechanism and ignition sensitivity of nanothermites. Materials Research Society Symposium Proceedings; Materials Research Society, 2006; pp 147−158.

(6) Wang, H.; Jian, G.; Egan, G. C.; Zachariah, M. R. Assembly and reactive properties of Al/CuO based nanothermite microparticles. *Combust. Flame* **2014**, *161*, 2203−2208.

(7) Wang, H.; DeLisio, J. B.; Jian, G.; Zhou, W.; Zachariah, M. R. Electrospray formation and combustion characteristics of iodine-containing Al/CuO nanothermite microparticles. *Combust. Flame* **2015**, *162*, 2823−2829.

(8) Monk, I.; Schoenitz, M.; Jacob, R. J.; Dreizin, E. L.; Zachariah, M. R. Combustion Characteristics of Stoichiometric Al-CuO Nanocomposite Thermites Prepared by Different Methods. *Combust. Sci. Technol.* **2017**, *189*, 555−574.

(9) Petrantoni, M.; Rossi, C.; Salvagnac, L.; Conédéra, V.; Estève, A.; Tenailleau, C.; Alphonse, P.; Chabal, Y. J. Multilayered Al/CuO thermite formation by reactive magnetron sputtering: Nano versus micro. *J. Appl. Phys.* **2010**, *108*, 084323.

(10) Zhou, X.; Shen, R.; Ye, Y.; Zhu, P.; Hu, Y.; Wu, L. Influence of Al/CuO reactive multilayer films additives on exploding foil initiator. *J. Appl. Phys.* **2011**, *110*, 094505.

(11) Blobaum, K. J.; Reiss, M. E.; Plitzko, J. M.; Weihs, T. P. Deposition and characterization of a self-propagating CuOx/Al thermite reaction in a multilayer foil geometry. *J. Appl. Phys.* **2003**, *94*, 2915−2922.

(12) Blobaum, K. J.; Wagner, A. J.; Plitzko, J. M.; Van Heerden, D.; Fairbrother, D. H.; Weihs, T. P. Investigating the reaction path and growth kinetics in CuOx/Al multilayer foils. *J. Appl. Phys.* **2003**, *94*, 2923−2929.

(13) Yu, C.; Zhang, W.; Hu, B.; Ni, D.; Zheng, Z.; Liu, J.; Ma, K.; Ren, W. Core/shell CuO/Al nanorod thermite film based on electrochemical anodization. *Nanotechnology* **2018**, *29*, 36LT02.

(14) Hu, B.; Zhang, W.; Yu, C.; Zheng, Z.; Chen, Y.; Wang, J.; Liu, J.; Ma, K.; Ren, W. Electrochemical Synthesis of Al/CuO Thermite Films on Copper Substrates. *Ind. Eng. Chem. Res.* **2019**, *58*, 7131−7138.

(15) Wang, Y.-t.; Zhang, X.-t.; Xu, J.-b.; Shen, Y.; Wang, C.-a.; Li, F.-w.; Zhang, Z.-h.; Chen, J.; Ye, Y.-h.; Shen, R.-q. Fabrication and characterization of Al−CuO nanocomposites prepared by sol-gel method. *Def. Technol.* **2020**, DOI: 10.1016/j.dt.2020.06.029.

(16) Calais, T.; Bancaud, A.; Estève, A.; Rossi, C. Correlation between DNA Self-Assembly Kinetics, Microstructure, and Thermal Properties of Tunable Highly Energetic Al-CuO Nanocomposites for Micropyrotechnic Applications. *ACS Appl. Nano Mater.* **2018**, *1*, 4716−4725.

(17) Shende, R.; Subramanian, S.; Hasan, S.; Apperson, S.; Thiruvengadathan, R.; Gangopadhyay, K.; Gangopadhyay, S.; Redner, P.; Kapoor, D.; Nicolich, S.; Balas, W. Nanoenergetic composites of CuO nanorods, nanowires, and Al-nanoparticles. *Propellants, Explos., Pyrotech.* **2008**, *33*, 122−130.

(18) Calais, T.; Bourrier, D.; Bancaud, A.; Chabal, Y.; Estève, A.; Rossi, C. DNA Grafting and Arrangement on Oxide Surfaces for Self-Assembly of Al and CuO Nanoparticles. *Langmuir* **2017**, *33*, 12193−12203.

(19) Umbrajkar, S. M.; Schoenitz, M.; Dreizin, E. L. Exothermic reactions in Al-CuO nanocomposites. *Thermochim. Acta* **2006**, *451*, 34−43.

(20) Stamatis, D.; Jiang, Z.; Hoffmann, V. K.; Schoenitz, M.; Dreizin, E. L. Fully dense, aluminum-rich Al-CuO nanocomposite powders for energetic formulations. *Combust. Sci. Technol.* **2008**, *181*, 97−116.

(21) Kwon, J.; Ducéré, J. M.; Alphonse, P.; Bahrami, M.; Petrantoni, M.; Veyan, J.-F.; Tenailleau, C.; Estève, A.; Rossi, C.; Chabal, Y. J. Interfacial chemistry in Al/CuO reactive nanomaterial and its role in exothermic reaction. *ACS Appl. Mater. Interfaces* **2013**, *5*, 605−613.

(22) Lanthony, C.; Guiltat, M.; Ducéré, J. M.; Verdier, A.; Hémeryck, A.; Djafari-Rouhani, M.; Rossi, C.; Chabal, Y. J.; Estève, A. Elementary surface chemistry during CuO/Al nanolaminate-thermite synthesis: Copper and oxygen deposition on aluminum (111) surfaces. *ACS Appl. Mater. Interfaces* **2014**, *6*, 15086−15097.

(23) Rossi, C. Engineering of Al/CuO Reactive Multilayer Thin Films for Tunable Initiation and Actuation. *Propellants, Explos., Pyrotech.* **2019**, *44*, 94−108.

(24) Marín, L.; Gao, Y.; Vallet, M.; Abdallah, I.; Warot-Fonrose, B.; Tenailleau, C.; Lucero, A. T.; Kim, J.; Esteve, A.; Chabal, Y. J.; Rossi, C. Performance Enhancement via Incorporation of ZnO Nanolayers in Energetic Al/CuO Multilayers. *Langmuir* **2017**, *33*, 11086−11093.

(25) Julien, B.; Cure, J.; Salvagnac, L.; Josse, C.; Esteve, A.; Rossi, C. Integration of Gold Nanoparticles to Modulate the Ignitability of Nanothermite Films. *ACS Appl. Nano Mater.* **2020**, *3*, 2562−2572.

(26) Kinsey, A. H.; Slusarski, K.; Sosa, S.; Weihs, T. P. Gas Suppression via Copper Interlayers in Magnetron Sputtered Al-Cu2O Multilayers. *ACS Appl. Mater. Interfaces* **2017**, *9*, 22026−22036.

(27) Yu, J.; McMahon, B. W.; Boatz, J. A.; Anderson, S. L. Aluminum Nanoparticle Production by Acetonitrile-Assisted Milling: Effects of Liquid- vs Vapor-Phase Milling and of Milling Method on Particle Size and Surface Chemistry. *J. Phys. Chem. C* **2016**, *120*, 19613−19629.

(28) Schoenitz, M.; Ward, T.; Dreizin, E. L. Preparation of Energetic Metastable Nano-Composite Materials by Arrested Reactive Milling. *MRS Proc.* **2011**, *800*, AA2.6.

(29) Williams, R. A.; Patel, J. V.; Dreizin, E. L. Ignition of Fully Dense Nanocomposite Thermite Powders by an Electric Spark. *J. Propul. Power* **2014**, *30*, 765−774.

(30) Mursalat, M.; Schoenitz, M.; Dreizin, E. L. Effect of premilling Al and CuO in acetonitrile on properties of Al·CuO thermites prepared by arrested reactive milling. *Combust. Flame* **2020**, *214*, 57−64.

(31) Gates-Rector, S.; Blanton, T. The Powder Diffraction File: a quality materials characterization database. *Powder Diffr.* **2019**, *34*, 352−360.

(32) Degen, T.; Sadki, M.; Bron, E.; König, U.; Nénert, G. The HighScore suite. *Powder Diffr.* **2014**, *29*, S13−S18.

(33) Huang, C.; Schoenitz, M.; Dreizin, E. L. Displacement of powders from surface by shock and plasma generated by electrostatic discharge. *J. Electrost.* **2019**, *100*, 103353.

(34) Huang, C.; Schoenitz, M.; Dreizin, E. L. Ignition of zirconium powders placed near an electrostatic discharge. *Combust. Flame* **2021**, *226*, 1−13.

(35) Fonseca, P. C.; Scherer, G. W. An image analysis procedure to quantify the air void system of mortar and concrete. *Mater. Struct.* **2015**, *48*, 3087−3098.

(36) Jiang, N.; Spence, J. C. H. Interpretation of oxygen K pre-edge peak in complex oxides. *Ultramicroscopy* **2006**, *106*, 215−219.

(37) Stamatis, D.; Ermoline, A.; Dreizin, E. L. A multi-step reaction model for ignition of fully-dense Al-CuO nanocomposite powders. *Combust. Theory Modell.* **2012**, *16*, 1011−1028.

(38) Zhang, S.; Dreizin, E. L. Reaction interface for heterogeneous oxidation of aluminum powders. *J. Phys. Chem. C* **2013**, *117*, 14025−14031.

(39) Mursalat, M.; Schoenitz, M.; Dreizin, E. L. Custom particle morphology in energetic nanocomposites prepared by arrested reactive milling in immiscible liquids. *Powder Technol.* **2020**, *359*, 238−246.

(40) Williams, R. A.; Schoenitz, M.; Ermoline, A.; Dreizin, E. L. On gas release by thermally-initiated fully-dense 2Al·3CuO nano-composite powder. *Int. J. Energ. Mater. Chem. Propul.* **2012**, *11*, 275−292.